Heliyon 10 (2024) e33062

Contents lists available at ScienceDirect

Heliyon

journal homepage: www.cell.com/heliyon

Research article

MiR-21 regulates skeletal muscle atrophy and fibrosis by targeting TGF-beta/SMAD7-SMAD2/3 signaling pathway

Xianmin Song [a,1], Fei Liu [a,1], Mengjie Chen [a,1], Minhui Zhu [a], Hongliang Zheng [a], Wei Wang [a], Donghui Chen [b,**], Meng Li [a,***], Shicai Chen [a,*]

[a] *From the Department of Otorhinolaryngology & Head and Neck Surgery, Changhai Hospital, Naval Military Medical University (The Second Military Medical University), Shanghai, 200433, China*

[b] *Department of Otorhinolaryngology, The First Affiliate Hospital of Nanjing Medical University, 300 Guangzhou Road, Nanjing, 210029, Jiangsu, China*

ARTICLE INFO

Keywords:
Skeletal muscle
Atrophic fibrosis
miR-21
SMAD7
SMAD2/3
Nuclear translocation

ABSTRACT

Long-term denervation-induced atrophy and fibrosis of skeletal muscle due to denervation leads to poor recovery of muscle function. Studies have shown that the transforming growth factor-β1 (TGF-β1)-Smad signaling pathway plays a central role in muscle atrophy and fibrosis. Recent studies demonstrate the role of microRNAs (miRs) in various pathological conditions, including muscle regeneration. miR-21 has been shown to play a dynamic role in inflammatory responses and in accelerating injury responses to fibrosis. We used both RNA sequencing and quantitative RT-PCR strategies to examine the alternations of miRNAs during denervation-induced gastrocnemius muscle atrophy and fibrosis. Our data showed that MiR-21 was upregulated in denervated gastrocnemius muscle tissue, and TGF-β1treatment increased miR-21 expression. Inhibition of miR-21 reduced gastrocnemius muscle fibrosis and significantly downregulated the expression of *p*-SMAD2/3 and the fibrosis-associated markers TGF-β1, connective tissue growth factor, alpha smooth muscle actin. Masson's trichrome staining revealed that atrophy and fibrosis in gastrocnemius muscle tissue were reduced in the miR-21 inhibition group compared to the control group. We confirmed that SMAD7 is a direct target of miR-21 using a dual luciferase assay. Furthermore, Immunofluorescence and Western blot analyses revealed that miR-21 inhibition reduced SMAD2/3 phosphorylation and nuclear translocation. While SMAD7-siRNA abolished the effect. Consequently, the discovery that miR-21 regulates the atrophy and fibrosis of the gastrocnemius muscle offers a possible therapeutic approach for their management.

* Corresponding author.
** Corresponding author.
*** Corresponding author.
E-mail addresses: dr_chendonghui@163.com (D. Chen), menglee198504@163.com (M. Li), docchen5775@163.com (S. Chen).
[1] These authors contributed equally to this work.

https://doi.org/10.1016/j.heliyon.2024.e33062
Received 11 December 2023; Received in revised form 12 June 2024; Accepted 13 June 2024
Available online 19 June 2024

1. Introduction

Poor recovery of muscle function in skeletal muscles following reinnervation was caused by long-term denervation-induced atrophy and fibrosis. Although microsurgical procedures have been employed in clinical settings with positive results, the functional recovery of injured skeletal muscle is still limited [1]. Because of atrophy and fibrosis resulting from excessive production and deposition of extracellular matrix (ECM), injured skeletal muscle cannot fully recover its biomechanical properties [2,3]. Fibrosis development hinders skeletal muscle regeneration, raises the risk of re-injury and reduces function [4,5].

Therefore, in order to enhance skeletal muscle healing following injury requires intervention against fibrosis. In various organ systems and tissues, the transforming growth factor-beta 1 (TGF-β1) signaling pathway is crucial in in regulating fibrosis [6]. Following nerve injury, satellite cells in skeletal muscle tissue produce TGF-β1, which affects fibroblasts and muscle cells through the autocrine and paracrine pathways. This results in the upregulation of connective tissue growth factor (CTGF) and several fibrosis-related proteins, including fibronectin, alpha smooth muscle actin (α-SMA), and type I and type III collagen, which are also important elements of the extracellular matrix [2,7]. TGF-β1 inhibits matrix metalloproteinase expression and decreases the breakdown of ECM components [8]. In addition, it directly induces myoblast dedifferentiation, suppresses myogenesis, and transforms myoblasts into fibroblasts, which produce a variety of fibrosis-related proteins [9]. Long-term denervated human laryngeal muscle exhibits higher expression of TGF-β1, which is positively correlated with both laryngeal muscle atrophy and ECM accumulation [10].

Short non-coding RNA sequences consisting of 20–23 nucleotides, known as microRNAs (miRNAs), cause mRNA degradation, which in turn suppresses the expression of protein-coding genes. According to earlier research, miRNA is essential to the pathophysiological mechanisms of multiple disorders, including muscular fibrosis. Previous studies have shown that miRNA plays a crucial role in the pathophysiological processes of various diseases such as muscle fibrosis. miRNAs such as miR-124a, miRNA-145 and miR-21 are involved in the fibrosis of various tissues and organs such as liver, lung, kidney and myocardium, where they influence the balance between ECM expression and degradation [11–13]. In skeletal muscle fibrosis, miRNAs may alter the TGF-β/Smad signaling pathway [14]. Targeting the TGF-β1 signaling pathway across multiple organs, miR-21 is a significant regulator of fibrosis [15,16]. However, the role and involvement of miR-21 in skeletal muscle fibrosis remain unclear and may be crucial in identifying viable therapeutic targets against skeletal muscle fibrosis.

In this study, we found that miR-21 expression is upregulated in denervated gastrocnemius muscle, suggesting that it may be involved in the pathological changes occurring in denervated gastrocnemius muscle. Our results suggest that miR-21 is involved in fibrosis of denervated laryngeal muscle by regulating the TGF-β1/Smad signaling pathway.

2. Materials and methods

2.1. Animals and the establishment of a mouse model of sciatic nerve injury

Eight-week-old male C57BL/6J mice were used in this study. All animal experimental procedures were carried out in accordance with the technical guidelines and approved by the Animal Care and Use Committee of the Second Military Medical University. Mice were anesthetized with sodium pentobarbital (Nembutal; 40 mg/kg intraperitoneal injection). We exposed the left sciatic nerve with a gluteus maximus split incision, resected a 10 mm segment of the nerve proximal to the bifurcation, and closed the skin. The right legs served as unoperated controls.

2.2. Generation of lentivirus-based RNAi plasmid

The mmu-miR-21–5p sequence was obtained from the miRBase database (http://www.mirbase.org). The lentivirus-based RNAi transfer plasmid pLKO0.1-puro-*anti*-miR-21 and the control plasmid pLKO.1-puro-NC were prepared using the pLKO.1-puro plasmid. To generate pLKO.1-puro-*anti*-miR-21, "CCGGT TAGCTTATCAGACTGATGTTGA G″ and "AATTC TCAACATCAGTCTGATAAGCTA A″ were prepared using 50 pmol forward and reverse oligonucleotides and 10× polymerase chain reaction (PCR) buffer (Takara Bio, Inc., Otsu, Japan) and cloned according to the U6 promoter into the *Age*I/*Eco*RI-digested pLKO.1-puro vector for the construction of pLKO.1-puro-*anti*-miR-21. The annealing conditions were as follows: 94 °C for 3 min; followed by 55 cycles at 80 °C for 30 s at −1 °C/cycle. The constructs were verified prior to use by sequencing by Sangon Biotech Co., Ltd. (Shanghai, China).

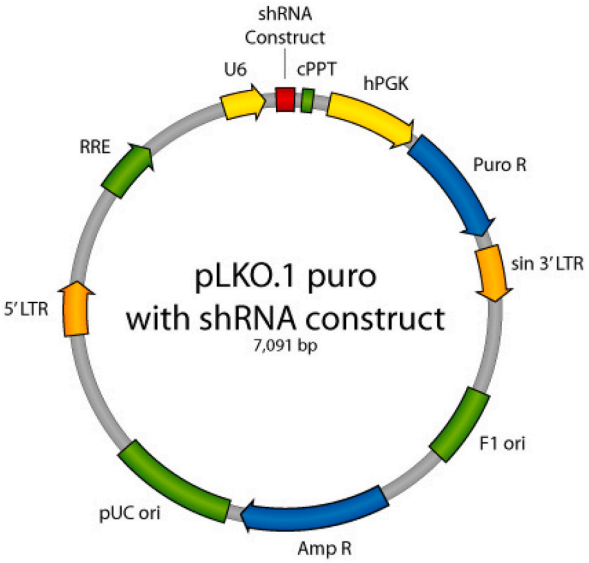

2.3. pLKO infection

After sciatic nerve injury, mice were randomly divided into groups (n ≥ 6). One day after surgery, mice were treated by intramuscular injections of pLKO-mimics-NC or pLKO-*anti*-miR-21 into the gastrocnemius muscle (10 μl/mouse/day, once every two days). At 1, 2, 3, and 4 weeks after surgery, mice were sacrificed and tissues were collected for analysis.

2.4. Masson's trichrome staining

Muscle tissue was fixed in 4 % paraformaldehyde for 24 h, dehydrated, and embedded in paraffin. 4 μm thick paraffin sections were cut. After deparaffinization and dehydration, sections were washed with distilled water and then stained with Masson's trichrome stain (Jiancheng Bioengineering Institute, Nanjing, China). Collagen-rich fibers were stained blue in the deformed area and the cell matrix was stained red. The images were taken under an optical microscope. Ten fields were randomly selected from each section. The images were captured and analyzed using Image J. The degree of fibrosis of the gastrocnemius muscle was expressed as the percentage of the area with fibrosis in the entire area.

2.5. Cell culture

HEK293T, C2C12 and NIH3T3 cells were purchased from Stem Cell Bank, Chinese Academy of Sciences, Shanghai, China. Cells were cultured at 37 °C with 5 % CO2 in Dulbecco's modified Eagle's medium supplemented with 10 % fetal bovine serum, penicillin, and streptomycin. Cells were subcultured every 2 days.

2.6. MicroRNA transfections

miR-21 mimics and inhibitors were synthesized by Genepharma (Shanghai, China). miR-21 mimics: 5′ uagcuuaucagacugauguuga 3′, anti-miR-21:5′ ucaacaucagucugauaagcua 3′, NC:5′ uuguacuacacaaaaguacug 3'. C2C12 cells were grown to ~70 % confluence and transfected in antibiotic-free media. They were then treated with 20 pmol of miR-21 mimetics, anti-miR-21 or NC using the transfection reagent Lipor Fiter (HB-RF-1000, Hanbio, China) for 6 h. The medium was then replaced with complete medium for 18 h.

2.7. Western blotting analyses

Tissues and cells were lysed with RIPA buffer containing proteinase and phosphatase inhibitors (Sigma, St. Louis, MO, USA). Protein concentration was determined with a bicinchoninic acid assay with bovine serum albumin (BSA) as a standard. Protein samples (50 μg) were loaded onto 10 % polyacrylamide gels, separated by sodium dodecyl sulfate–polyacrylamide gel electrophoresis, and then electrotransferred onto nitrocellulose membranes. The membranes were blocked with 10 % non-fat milk in Tris-buffered saline for 1 h and incubated overnight at 4 °C with anti-SMAD2/3 (1:1000; #5678, Cell Signaling Technology, Danvers, MA, USA), anti-*p*-SMAD-2/3 (1:1000; #8828, Cell Signaling Technology), anti-SMAD-7 (1 μg/mL; MAB2029-SP, R&D Biotechnology, Minneapolis, MN, USA), anti-TGF-β1 (1:500; MAB1835-SP, R&D Biotechnology), anti-CTGF (1:1000; MAB91901-SP, R&D Biotechnology), anti-α-SMA (1:1000; A5228, Sigma), anti-GAPDH (1; 1000; AF0006,Beyotime Biotechnology, Shanghai, China) antibodies diluted in phosphate-buffered

saline (PBS) with 1 % BSA. The membranes were then incubated with alkaline phosphatase-conjugated goat anti-rabbit IgG (Sigma) or goat anti-mouse IgG (Sigma) diluted 1:5000 in 2 % BSA in PBS for 1 h at room temperature. Western blot protein bands were visualized with chemiluminescent HRP substrate (WBKLS0050; Millipore, Bedford, MA, USA).

2.8. QRT-PCR

Muscle tissue and cells were homogenized in 1 mL Trizol reagent (Invitrogen, Carlsbad, CA, USA). Total RNA was extracted with chloroform, precipitated with isopropanol, and resuspended in 50 μL RNase-free water. We determined the concentration of isolated total RNA by measuring the optical density at A260 nm with a Nanodrop 1000 spectrophotometer (Thermo Fisher Scientific, Waltham, MA, USA).

Reverse transcription of 1 μg of total RNA was performed to synthesize cDNA using a PrimerScript™ RT reagent kit (TaKaRa Biotechnology, Dalian, China) in a GeneAmp PCR System 9700 (Applied Biosystems, Foster City, CA, USA). The primer sequences used are listed in Table 1.

qRT-PCR was performed using a SYBR® Premix Ex Tag™ II Kit (TaKaRa, Shiga, Japan). Reactions were carried out in 20 μL volumes with 0.5 μL cDNA. The amplification program consisted of an initial denaturation step at 95 °C for 2 min, followed by 40 cycles of denaturation at 95 °C for 15 s, annealing at 60 °C for 10 s, and elongation at 72 °C for 10 s with a final elongation step at 72 °C for 10 min. Data were collected and analyzed using a Rotor-Gene Q real-time PCR cycler (Qiagen, Doncaster, Victoria, Australia). We assessed the specificity of the PCR products by measuring the melting curves of the reactions. We analyzed the relative expression of target genes using the quantitative 2-ΔΔCT method and normalized to 18S rRNA.

2.9. Dual luciferase reporter gene assay

A dual-luciferase reporter gene assay was used to examine whether SMAD7 was the direct target gene of miR-21. The SMAD7 gene was inserted into the pmirGLO plasmid (Promega, Madison, WI, USA). Wild-type (wt) and mutant-type (mut) luciferase reporter plasmids were confirmed by sequencing and co-transfected with miR-21 into HEK293T cells. After 48 h, the transfected cells were harvested, lysed, centrifuged for 3–5 min, and the supernatant was collected.

A luciferase assay kit (RG005; Beyotime Biotechnology) was used to dissolve Renilla luciferase detection buffer solution and firefly luciferase detection agent, respectively. The Renilla luciferase working solution consisted of 100 μL buffer solution mixed with the Renilla luciferase substrate at a ratio of 1:100. We then measured 20–100 μL of samples from each group using a fluorimeter and then mixed the samples with 100 μL of firefly luciferase detection agent using a pipette. The reporter gene cell lysate was used as a blank control. The samples were mixed with 100 μL of luciferase working solution and the luciferase activity was measured with a

Table 1
Primer sequences used for qRT-PCR.

Name	Seqence (5'-3')
SMAD7 primer-F	5′AAACTAGCGGCCGCTAGTTG3′
SMAD7 primer-R	5′AGATCTAGCTTATGTTAAAGTTT3′
TGFβ1 primer-F	5′AAACTAGCGGCCGCTAGTAG3′
TGFβ1 primer-R	5′AGATCTAGCTTATAATGATGGTTT3′
α-SMA primer-F	5′-AACACGGCATCATCACCAAC-3′
α-SMA primer-R	5′-CACAGCCTGAATAGCCACATAC-3
GAPDH primer-F	5′-ATCACTGCCACCCAGAAG-3
GAPDH primer-R	5′-TCCACGACGGACACATTG-3′
U6 primer-F	5′-CTCGCTTCGGCAGCACA-3′
U6 primer-R	5′-AACGCTTCACGAATTTGCGT-3′
CTGF primer-F	5′-GGACACGAACTCATTAGAC-3′
CTGF primer-R	5′-TCTCACTTTGGTGGGATAG-3′
miR-181 primer	5′CTCGAGTAGAGATTGCAACGCTCTTTTA3′
miR-410 primer	5′AGGTrGTCTGTGATGAGTTCG3′
miR-302d primer	5′GGGACTTTGTGCGATTGGT3′
miR-551 primer	5′AAGTGGACCAGGTGATCGGC3′
miR-877 primer	5'TGCGGGTGCTCGCTTCGGCAGC3'
miR-340 primer	5′GCGGTTATAAAGCAATGAGA3′
miR-412 primer	5′CTCAACTGGTGTCGTGGAGTCGGCAATT3′
miR-322 primer	5′ AATAAAGCTTACCCGGGTCAATAAATGAAA3′
miR-744 primer	5′AATGCGGGGCTAGGGCTA3′
miR-200 primer	5′TAATACTGTTGGGTAATGATGGA3′
miR-329 primer	5′GGGAACACACCTGGTTAAC3′
miR-17 primer	5′ACTACCTGCACTGTAAGCACTTTGCCAGAG3′
miR-326 primer	5′GGCAAATGTCAGAGGGTT3′
miR-15b primer	5′AGGUGCAATCGGTGTTCA3′
miR-26a primer	5′TTCAA GTAATCCAGG ATAGG CT3′
miR-155 primer	5′GCTACTCGAGCCTTTCAGATTTACTATATGC3′
miR-15a primer	5′CGCCTAGCAGCACATAATGG3′

fluorimeter. Renilla luciferase was used as a control. Relative luciferase activity was calculated as relative luciferase units (RLU) of firefly luciferase/RLU-Renilla luciferase.

2.10. Immunofluorescence

Mice were fixed by transcardial perfusion with 4 % paraformaldehyde in 0.1 M phosphate buffer (PB), pH 7.4. The gastrocnemius samples were dissected and cryoprotected with 30 % sucrose in PBS (pH 7.4) overnight at 4 °C. Cryosections with a thickness of 7 μm

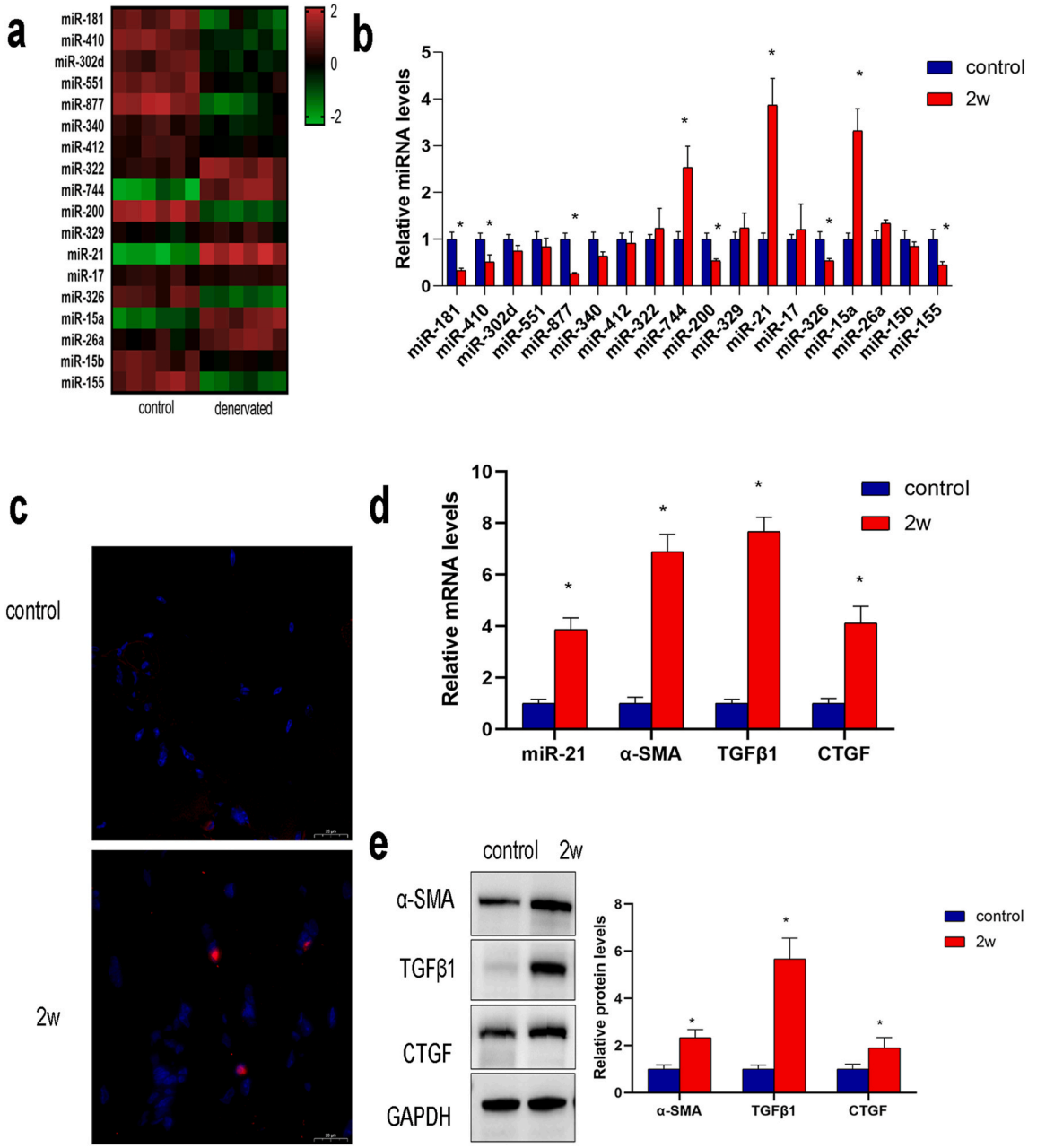

Fig. 1. miR-21 expression is upregulated in denervated mouse gastrocnemius muscles a) Heat map of 18 different miRNAs in denervated mouse gastrocnemius muscles and normal gastrocnemius muscles (n = 6). b) qRT-PCR analysis of the expression of microRNA expression in denervated gastrocnemius muscle relative to normal tissue,n = 6,*P < 0.05. c) In situ hybridization of miR-21 expression levels in denervated mouse gastrocnemius muscles and normal gastrocnemius muscles, scale bar = 20um. d) qRT-PCR analysis of the expression of TGF-β1, α-SMA and CTGF ingastrocnemius muscle tissue 2 weeks after denervation, n = 6, *P < 0.05. e) Western blot and quantitative analysis (right) of TGF-β1, α-SMA and CTGF in gastrocnemius muscle tissue 2 weeks after denervation, n = 6, *P < 0.05.

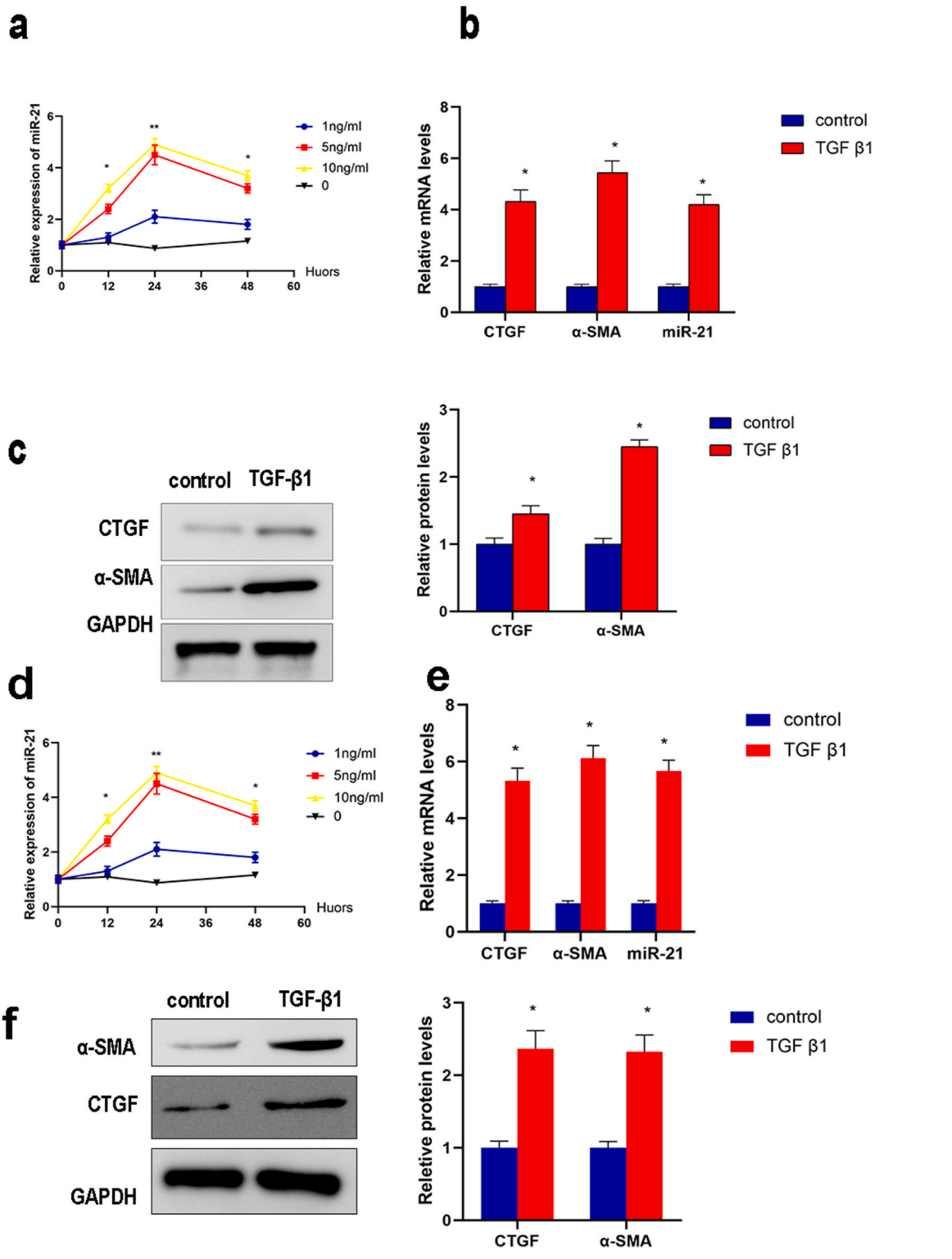

(caption on next page)

Fig. 2. TGF-β1 up-regulated expression of miR-21 in C2C12 cells, which correlates with α-SMA and CTGF expression a) qRT-PCR analysis of the expression of miR-21 in C2C12 cells 0,12h,24h,48h after treatment of TGF-β1; n = 6, *P < 0.05. b) qRT-PCR analysis of the expression of CTGF, α-SMA and miR-21 in C2C12 cells 24 h after treatment of TGF-β1compared with control; n = 6, *P < 0.05. c) Western blot and quantitative analysis of CTGF and α-SMA in C2C12 cells 24 h after treatment of TGF-β1; n = 6, *P < 0.05. d) qRT-PCR analysis of the expression of miR-21 in NIH3T3 cells 0,12h,24h,48h after treatment of TGF-β1; n = 6, *P < 0.05. b) qRT-PCR analysis of the expression of CTGF, α-SMA and miR-21 in NIH3T3cells 24 h after treatment of TGF-β1compared with control; n = 6, *P < 0.05. c) Western blot and quantitative analysis of CTGF and α-SMA in NIH3T3 cells 24 h after treatment of TGF-β1.

were permeabilized for 1 h by incubation with 0.1 M PB (pH 7.4) containing 0.3 % Triton X-100 and 10 % goat serum (PBTGS). Sections were incubated with antibodies against CTGF (1:200, R&D Biotechnology), α-SMA (1:100, Sigma), or SMAD2/3 (1:1000; Cell Signaling Technology, Danvers, MA, USA) overnight at 4 °C. Next, the samples were washed three times and incubated with a secondary antibody (Jackson Immuno Research Laboratories, Inc., West Grove, PA, USA) for 1 h at 37 °C, and counterstained with DAPI (Sigma Aldrich Inc.) before mounting. Five random fields of each sample were photographed under a leica DL2000 fluorescence microscope.

2.11. miRNA ISH

The gastrocnemius samples were fixed in 4 % paraformaldehyde for 10 min, then treated with 5 mg/mL proteinase K (Sigma-Aldrich, Budapest, Hungary). Then they were acetylated by incubation in acetic anhydride/triethanolamine and pre-hybridized in a hybridization solution (50 % formamide, 0.3 M sodium-chloridep (H 7.0), 20 mM Tris-HCl, 5 mM ethylenediaminetetraacetic acid, 1 × Denhardt's solution, and 0.5 mg/mL yeast tRNA) for 4 h. The samples were incubated in pre-hybridization buffer for 1 h at 37 °C, then hybridized with 8 ng/μL digoxigenin-labeled miR-21 oligonucleotide probes (5'TCAACATCAGTCTGATAAGCTA3') (Sangon Biotech, Shanghai, China) overnight at 37 °C. The hybridized samples were washed sequentially in 2 × , 1 × , and 0.5 × saline-sodium citrate, then incubated with mouse anti-digoxigenin horseradish peroxidase antibody (1:500; PerkinElmer, Per-Form Hungary, Budapest, Hungary). Finally, the samples were stained with 3,3′-diaminobenzidine, dehydrated, and observed under a microscope.

2.12. Statistical analyses

All experiments were performed in triplicate. Experimental data are presented as means ± standard errors of the mean and were analyzed using one-way analysis of variance and Dunnett's t tests. Values were considered significantly different at $P < 0.05$.

3. Results

3.1. miR-21 expression is increased in denervated mouse gastrocnemius muscles

miRNA microarrays were used to identify miRNA expressions in denervated mouse gastrocnemius muscles at the early stage of denervation (2 weeks after denervation). The microarray data showed that the expression of several miRNAs (miR-181, miR-410, miR-302d, miR-551, miR-877, miR-340, miR-412, miR-322, miR-744, miR-200, miR-329, miR-21, miR-17, miR-326, miR-15b, miR-26a, miR-155, and miR-15a) was altered in denervated gastrocnemius muscle compared to normal muscle tissue. The most notable changes were observed for miR-21, with a 4-fold upregulation compared to control (n = 6, *p < 0.05; Fig. 1a and b). Furthermore, previous research has indicated a role for miR-21 in fibrosis; for these reasons, miR-21 was selected for additional investigation. Using quantitative real-time PCR (qRT-PCR), we found that among the differentially expressed miRNAs miR-21 expression was significantly higher in denervated gastrocnemius muscle compared to normal muscle tissue (n = 6,*P < 0.05; Fig. 1b), in situ hybridization (ISH) for miR-21 demonstrated that miR-21 expression was increased in gastrocnemius muscle 2 weeks after denervation (Fig. 1c). To further explore the relationship between miR-21 expression and gastrocnemius muscle fibrosis, we examined the expression of key fibrosis markers such as: TGF-β1, α-SMA and CTGF. QRT-PCR and western blotting analyses revealed that the expression of TGF-β1, α-SMA and CTGF was significantly higher 2 weeks after denervation (n = 6, *P < 0.05; Fig. 1d and e). The temporal changes in miR-21 expression correlated with those of TGF-β1, α-SMA and CTGF. Collectively, these results indicate that miR-21 expression is associated with the development of fibrosis.

3.2. miR-21 expression is upregulated in cells stimulated with TGF-β1

To identify the role that miR-21 plays in fibroblast, we stimulated C2C12 and NIH3T3 cells with TGF-β1 for 12, 24, or 48 h. Untreated cells were examined as controls. TGF-β1 stimulation up-regulated miR-21 expression level, which correlated with an increase in α-SMA and CTGF at both mRNA and protein levels (TGF-β1, 5 ng/mL, 24 h) (Fig. 2(a-f)).

3.3. miR-21 promotes fibrosis changes in C2C12 cells

To explore the role of miR-21 in cells, we transfected C2C12 and NIH3T3 cells with miR-21 mimics, negative control (NC) and anti-miR-21. Compared with the (NC), the expression level of miR-21 increased and decreased significantly in miR-21 mimetics and anti-miR-21 group, respectively (n = 6, *P < 0.05; Fig. 3a–d). The expression of CTGF and α-SMA in both cells was examined by qRT-PCR,

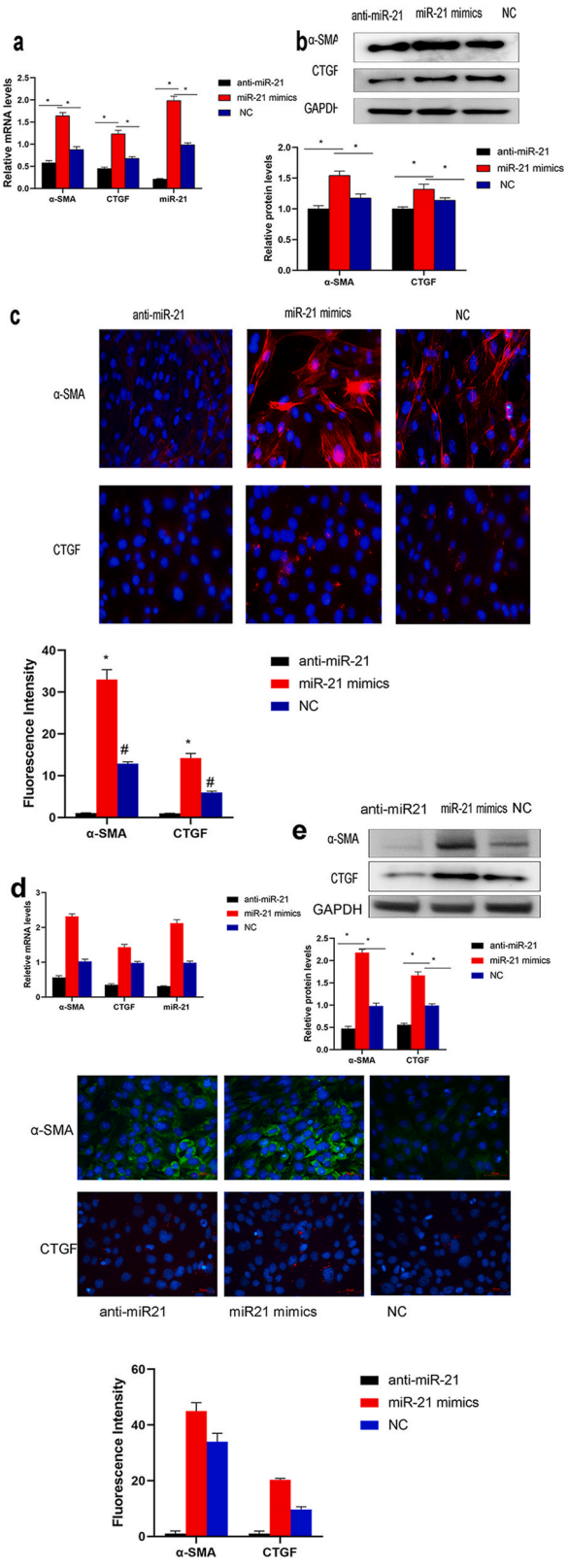

(caption on next page)

Fig. 3. The effects of miR-21 on fibrosis-related protein expression in vitro a) mRNA expression of α-SMA and CTGF in C2C12 cells transfected with anti-miR-21, NC, or miR-21 mimics; *P < 0.05. b) Western blots showing the expression of α-SMA and CTGF in C2C12 cells transfected with anti-miR-21, NC, or miR-21 mimics. Bar graphs showing the quantified Western blotting results normalized to GAPDH; *P < 0.05. c) Immunofluorescence staining of α-SMA and CTGF protein in C2C12 cells transfected with anti-miR-21, NC, or miR-21 mimics. d) mRNA expression of α-SMA and CTGF in NIH3T3 cells transfected with anti-miR-21, NC, or miR-21 mimics; *P < 0.05. e) Western blots showing the expression of α-SMA and CTGF in NIH3T3 cells transfected with anti-miR-21, NC, or miR-21 mimics. Bar graphs showing the quantified Western blotting results normalized to GAPDH; *P < 0.05. f) Immunofluorescence staining of α-SMA and CTGF protein in NIH3T3 cells transfected with anti-miR-21, NC, or miR-21 mimics, scale bar = 50um.

western blotting, and immunofluorescence staining. Compared with the NC group, the gene expressions of α-SMA and CTGF were significantly increased in the miR-21 mimics group (n = 6, *P < 0.05, Fig. 3). Treatment with anti-miR-21 reversed the changes. (Fig. 3 (a-f)).

3.4. Knockdown of miR-21 attenuated the fibrosis of denervated muscles

To observe the effect of miR-21 on gastrocnemius muscle fibrosis. We injected the pLKO-*anti*-miR-21 or pLKO-NC vectors into the gastrocnemius muscles of mice (n = 6) every other day after sciatic nerve injury. We detected the expression of miR-21 by qPCR at different time points (0, 1W, 2W, 3W, 4W) after denervation. We found that the expression of miR-21 increased significantly after denervation and peaked at 2 weeks after denervation (Fig. 4a, n = 6, #P < 0.05, compared with control). Compared to the pLKO-NC group, the expression of miR-21 was significantly reduced in the pLKO-*anti*-miR-21 group (Fig. 4a, n = 6, *P < 0.05). The mRNA and protein levels of CTGF and α-SMA in the pLKO-*anti*-miR-21 group were significantly lower than those in the pLKO-NC group. (Fig. 4b–d, n = 6, #P < 0.05, compared to control, n = 6, *P < 0.05, compared to pLKO-NC group). Masson's trichrome staining for fibrosis showed a significant increase in fibrosis in the gastrocnemius muscles 4 weeks after denervation compared to control. Muscle fibrosis was attenuated in the pLKO-*anti*-miR-21 group compared to the pLKO-NC group (Fig. 4e–f, n = 6, #P < 0.05 compared to control, n = 6, *P < 0.05 compared to pLKO-NC group). Immunofluorescence staining revealed that pLKO-*anti*-miR-21 treatment reduced the expression of CTGF and α-SMA at week 2 after denervation (Fig. 4g).

3.5. SMAD7 is a direct target of miR-21

In vivo studies showed that SMAD7 was inhibited in the pLKO-NC group, while pLOKO-*anti*-miR-21 could reverse protein expression (Fig. 5a and b). Previous studies clearly demonstrated that SMAD7 had an 8-nucleotide miR-21 binding site in its 3′-untranslated region (Li et al., 2013; Lin et al., 2014). To investigate whether miR-21 can repress the expression of SMAD7 by binding to its 3′-UTR, we created a luciferase reporter vector containing the SMAD7 3′-UTR together with a vector expressing miR-21. co-transfected into HEK293T cells. A dual-luciferase reporter assay was performed. miR-21 significantly inhibited the luciferase activity of SMAD7 compared to the NC group (Fig. 5c, *P < 0.05). To investigate the effects of miR-21 on SMAD7 in C2C12 cells, we performed qRT-PCR and Western blot analyzes to determine the expression of related genes. SMAD7 levels decreased after transfection with miR-21 mimetics (Fig. 5d–f). In summary, our results suggest that SMAD7 is a direct target of miR-21.

3.6. miR-21 promotes fibrosis by TGF-beta/SMAD7-SMAD2/3 pathway

To investigate the role of SMAD7 in miR-21-mediated cell fibrosis, we transfected a SMAD7 siRNA together with a miR-21 inhibitor into C2C12 and NIH3T3 cells. Western blot and qRT-PCR analyzes revealed that the miR-21 inhibitor caused a decrease in α-SMA and CTGF expression. While SMAD7 siRNA reversed the effect of miR-21 inhibitor (Fig. 6a–c, Fig. 7a–c). The results showed that the miR-21 inhibitor treatment group had significantly reduced phosphorylation of the increased expression level of SMAD2/3 of SMAD7, which was reversed by co-transfection with SMAD7 siRNA (Fig. 6d and e, Fig. 7d and e). To detect the nuclear translocation of SMAD2/3, the nuclear and cytoplasmic proteins were extracted after drug treatment using the NE-PER nuclear and cytoplasmic extraction reagents. Western blot showed that cytoplasmic SMAD2/3 levels increased while nuclear SMAD2/3 levels decreased in the miR-21 inhibitor treatment group, which was reversed by co-transfection with SMAD7 siRNA (Fig. 6f and g). Immunofluorescence showed that SMAD2/3 nuclear translocations induced by miR-21 inhibitor were inhibited by SMAD7 siRNA treatment (Fig. 6h and I, Fig. 7f and g). Furthermore, an in vivo study showed that in the pLKO-NC group, SMAD7 was inhibited and the phosphorylation levels of SMAD2/3 were higher than in the sham group, while pLKO-*anti*-miR-21 could reverse the protein expression (Fig. 6j).). All these results indicate that the effect of miR-21 on promoting gastrocnemius muscle fibrosis was achieved through the inhibition of SMAD7 and other factors.

Western blots showing the expression of SMAD2/3 in the nuclear in NIH3T3cells transfected with anti-miR-21 with or without SMAD7 siRNA. g) Bar graphs represent quantifications of the Western blotting bands relative to LamniB1 expression; n = 6, *P < 0.05. h) Distributional changes SMAD2/3 were assessed by imunostaining bar = 50 μm). i) Western blots showing smad2/3 psmad2/3 and smad7 protein expression in gastrocnemius muscles of denervated mice.

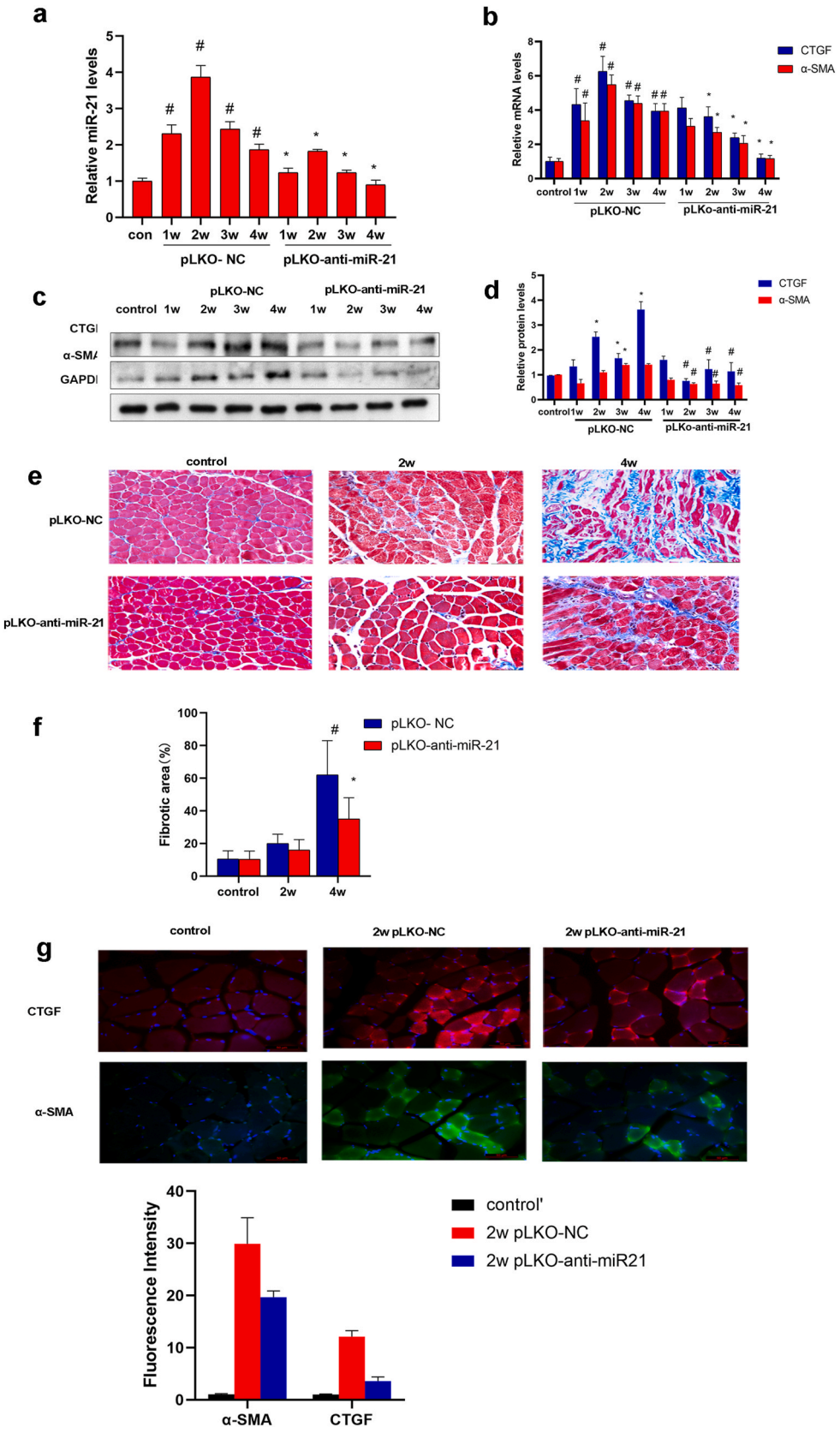

(caption on next page)

Fig. 4. The effects of miR-21 on fibrosis-related protein expression in vivo a) qRT-PCR analysis of the expression of miR-21 in gastrocnemius muscles of denervated mice (n = 6,#P < 0.05,compared with control; *P < 0.05 compared with pLKO- NC group); b) qRT-PCR analysis of the expression of CTGF and α-SMA in gastrocnemius muscles of denervated mice (n = 6,#P < 0.05,compared with control; *P < 0.05 compared with pLKO- NC group); c) Western blots showing CTGF, and α-SMA protein expression in gastrocnemius muscles of denervated mice. d)Bar graphs depicting the quantified Western blotting bands shown in c) by densitometry and normalized to GAPDH expression; (n = 6,#P < 0.05,compared with control; *P < 0.05 compared with pLKO- NC group); e) Masson's trichrome staining of gastrocnemius muscles harvested 2 and 4-weeks post-denervation, scale bar = 20um. f) Quantification of gastrocnemius muscle fibrosis in the indicated groups of mice (n = 6,#P < 0.05,compared with control; *P < 0.05 compared with pLKO- NC group). g) Immunofluorescence staining of CTGF, and α-SMA in gastrocnemius muscles of denervated mice, scale bar = 50um (2 weeks after denervation).

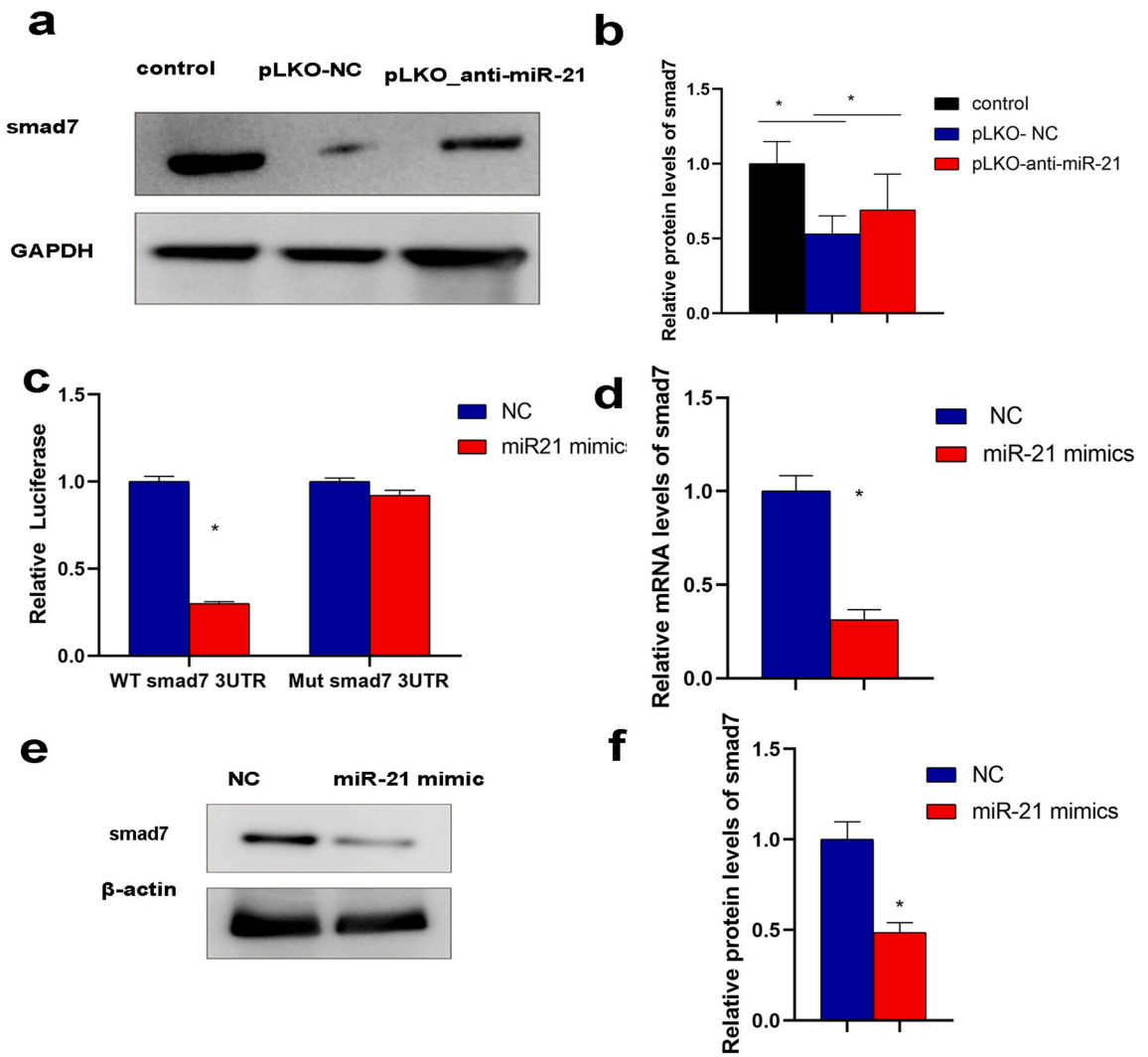

Fig. 5. SMAD7 is a direct target of miR-21 a) Western blots showing the expression of SMAD7 protein in the muscles of denervated mice (2 weeks after denervation). b) Bar graphs represent quantifications of the Western blotting bands by densitometry relative to β-actin expression; n = 6, *P < 0.05. c) Luciferase reporter assays in HEK293T cells co-transfected with miR-21 and either WT smad7 3′-UTR or Mut smad7 3′-UTR. d) mRNA expression of Smad7 in C2C12 cells transfected with miR-21 mimics or NC; n = 6, *P < 0.05. e) Western blots showing the expression of Smad7 protein in C2C12 cells transfected with miR-21 mimics or NC. f) Bar graphs represent quantifications of the Western blotting bands by densitometry relative to β-actin expression; n = 6, *P < 0.05.

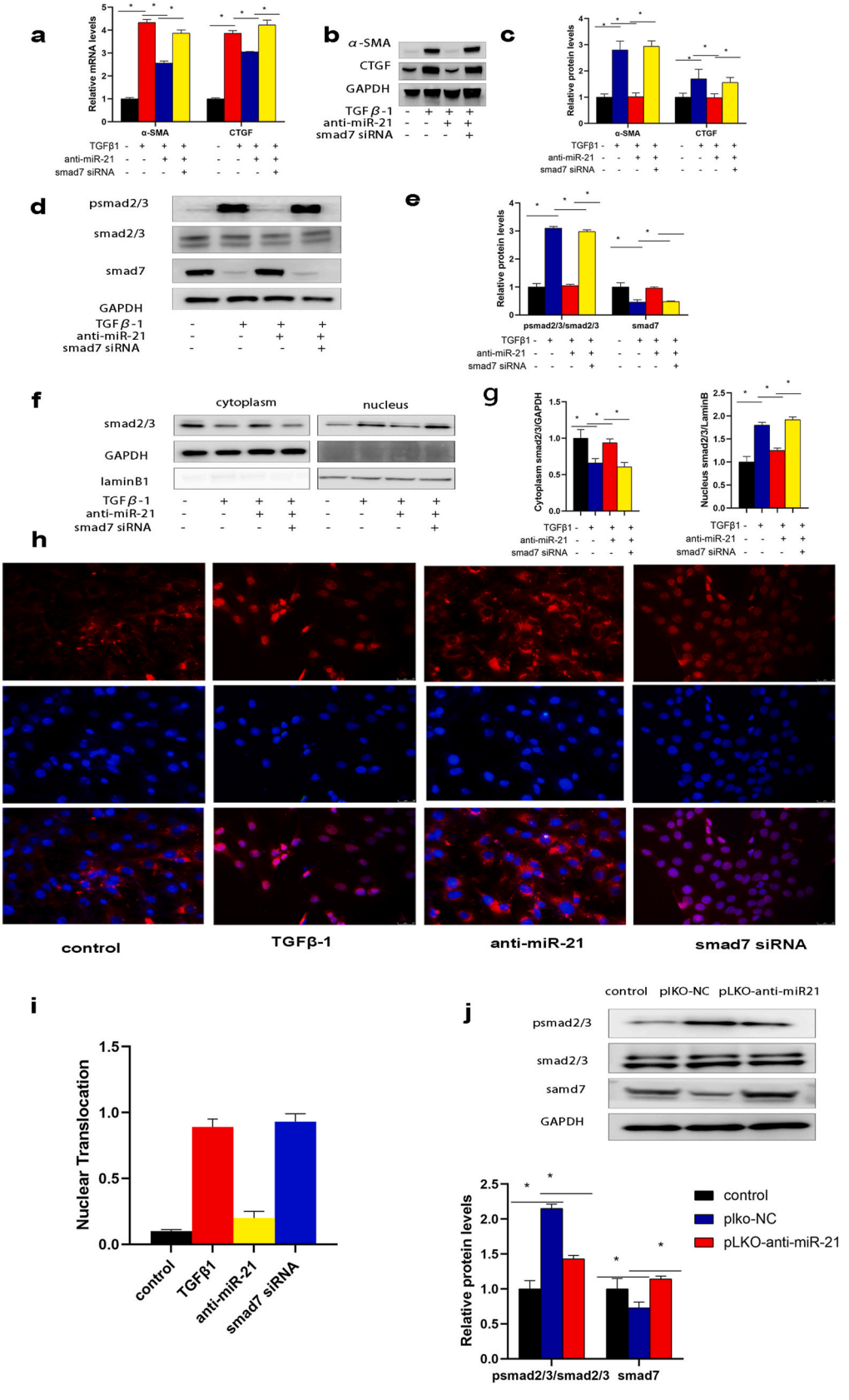

(caption on next page)

Fig. 6. miR-21 promotes fibrosis by suppressing the SMAD7 signaling pathway in C2C12 cells a) mRNA expression of CTGF and α-SMA in C2C12 cells transfected with anti-miR-21 with or without SMAD7 siRNA; n = 6, *P < 0.05. b) Western blots showing CTGF and α-SMA expression in C2C12 cells transfected with anti-miR-21 with or without SMAD7 siRNA. c) Bar graphs represent quantifications of the Western blotting bands relative to GAPDH expression; *n = 6, P < 0.05. d) Western blots showing the expression of *p*-SMAD2/3, SMAD2/3, and SMAD7 in the cytoplasm in C2C12 cells transfected with anti-miR-21 with or without SMAD7 siRNA. e) Bar graphs represent quantifications of the Western blotting bands relative to GAPDH expression; n = 6, *P < 0.05. f) Western blots showing the expression of SMAD2/3 in the nuclear in C2C12 cells transfected with anti-miR-21 with or without SMAD7 siRNA. g) Bar graphs represent quantifications of the Western blotting bands relative to LamniB1 expression; n = 6, *P < 0.05. h) Distributional changes SMAD2/3 were assessed by imunostaining bar = 50 μm). i) Bar graphs represent nuclear translocation of smad2//3. j)Western blots showing smad2/3 psmad2/3 and smad7 protein expression in gastrocnemius muscles of denervated mice.

4. Discussion

Muscle denervation caused by nerve injury leads to the derangement of muscle structure and functional changes. Muscle fibrosis represents a major obstacle to the success of muscle regeneration after nerve repair [17–21]. However, there is still no successful treatment to reduce skeletal muscle fibrosis after denervation. Therefore, in the present study, we created mouse models of gastrocnemius muscle fibrosis and identified the role of miR-21 in gastrocnemius muscle fibrosis after denervation. Our results showed that

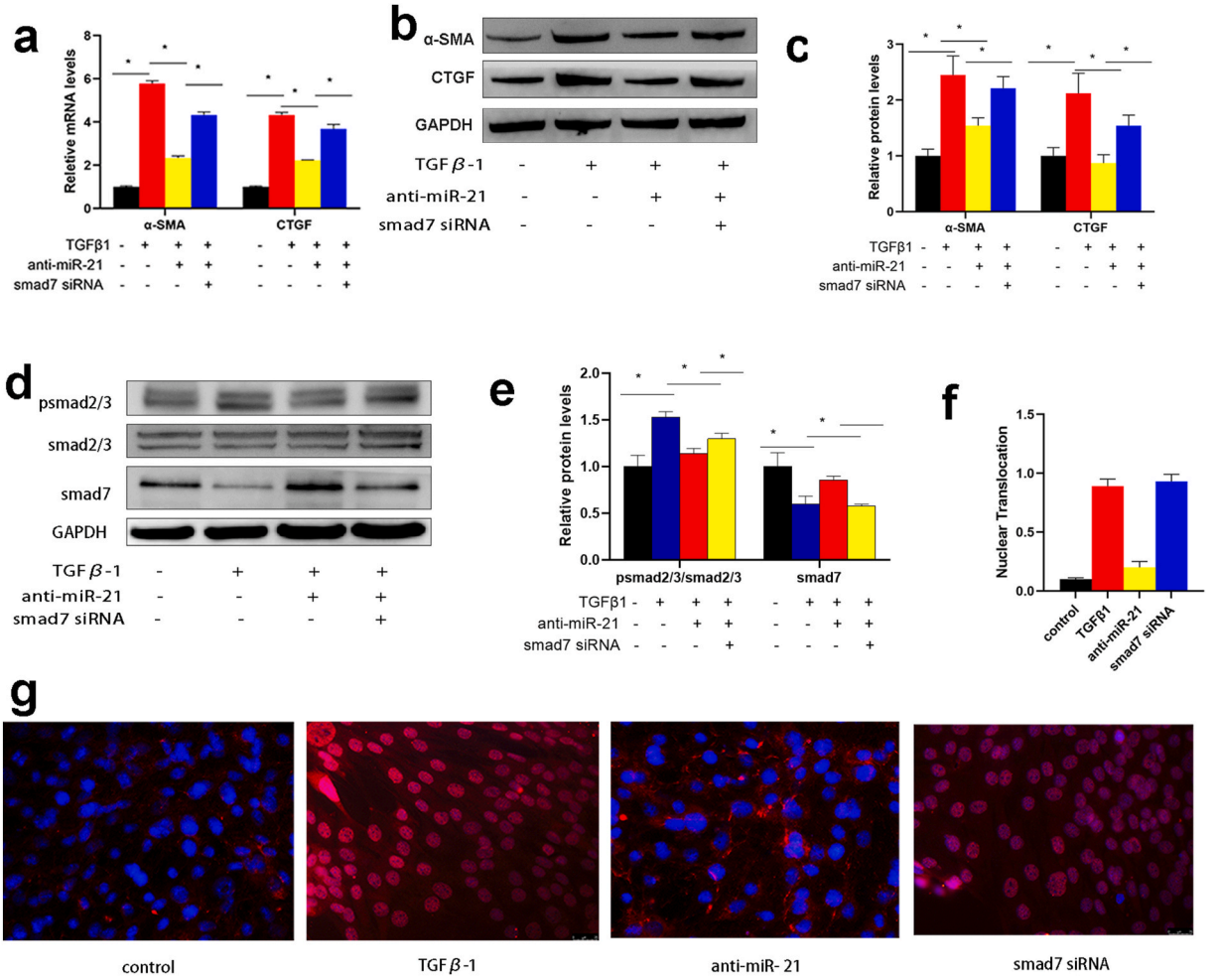

Fig. 7. miR-21 promotes fibrosis by suppressing the SMAD7 signaling pathway in NIH3T3 cells a) mRNA expression of CTGF and α-SMA in NIH3T3cells transfected with anti-miR-21 with or without SMAD7 siRNA; n = 6, *P < 0.05. b) Western blots showing CTGF and α-SMA expression in NIH3T3cells transfected with anti-miR-21 with or without SMAD7 siRNA. c) Bar graphs represent quantifications of the Western blotting bands relative to GAPDH expression; *n = 6, P < 0.05. d) Western blots showing the expression of *p*-SMAD2/3, SMAD2/3, and SMAD7 in the cytoplasm in NIH3T3 cells transfected with anti-miR-21 with or without SMAD7 siRNA. e) Bar graphs represent quantifications of the Western blotting bands relative to GAPDH expression; n = 6, *P < 0.05. f). Bar graphs represent nuclear translocation of smad2//3. g) Distributional changes SMAD2/3 were assessed by imunostaining bar = 50 μm).

miR-21 is significantly upregulated in gastrocnemius muscle fibrosis and that treatment with miR-21 inhibitors would reduce muscle fibrosis and prevent muscle dysfunction. This anti-fibrosis effect of the inhibitor was confirmed by an in vitro study with C2C12 cells, which showed that miR-21 is an important regulator of fibrosis.

Multiple evidences have shown that miRNAs are involved in various diseases, including cancer, inflammation, autoimmune diseases, and muscle denervation, and treatment targeting microRNAs is considered a promising approach [22–26]. miR-21 is abundantly expressed in numerous tissues and cells. miR-21 plays an important role in regulating fibrosis in several tissues, such as the kidneys, liver, lungs and muscle tissue [27–31]. However, the role of miR-21 in the development of fibrosis is controversial, with some studies showing that miR-21 promotes fibrosis, but others showing no influence [31–35]. Similar to previous studies, our study also showed that overexpression of miR-21 using miR-21 mimics enhanced the α-SMA and CTGF upregulatory effects of TGF-β1, whereas inhibition of miR-21 partially reversed the effects of TGF-β1. This suggests that miR-21 promotes gastrocnemius muscle fibrosis. However, the function and involvement of miR-21 in skeletal muscle fibrosis after denervation remains unclear.

Several signaling pathways are involved in miR-21-mediated fibrosis, including the TGF-β1/SMAD, ERK/NF-kB, PTEN/AKT, and IL-13/SMAD signaling pathways [36–40]. In this study, we found that treatment with miR-21 inhibitor increased the expression of SMAD7 in vitro and in vivo, suggesting a regulatory role of miR-21 in TGF-β1–SMAD7 signaling. We confirmed that miR-21 could simultaneously target SMAD7 through dual-luciferase reporter assays, which is consistent with previous studies [41–44]. SMAD7, an inhibitor of SMAD-2/3 phosphorylation [45], is an essential negative regulator in the TGF-β1/Smad signaling pathway and inhibits fibrosis by regulating this pathway [46–48].

The fibrosis effects of TGF-β1 are mainly mediated by the SMAD2/3-dependent pathway [49]. TGF-beta1 was previously shown to mediate activation of SMAD2/3 and then activated SMAD2/3 binds to SMAD4 to form a complex that translocates to the nucleus and regulates specific genes [50]. As expected, overexpression of miR-21 resulted in overactivation of the SMAD2/3 signaling pathway and caused fibrosis, but miR-21 inhibitors reversed this phenomenon. We found that miR-21 inhibitors inhibited TGF-β1-induced SMAD2/3 phosphorylation and nuclear translocation. Furthermore, we silenced the SMAD7 gene using siRNA, which resulted in an increase in nuclear translocation of *p*-SMAD2/3 and SMAD2/3. This demonstrates that the effect of miR-21 on promoting gastrocnemius muscle fibrosis was achieved through inhibiting SMAD7 and thereby activating the TGF-β/SMAD2/3 signaling pathway.

Functionally, miR-21 has been assigned a variety of activities. Its therapeutic inhibition demonstrated efficacy in a wide range of preclinical models of tissue fibrosis. The potential of miR-21 as a biomarker and therapeutic target has been highlighted [51]. Consequently, a direct miR-21 inhibitor (RG-012) has already passed clinical phase I and is now being tested in a phase II study in renal fibrosis. Consistent with other studies, our study suggested that miR-21 inhibitors may be useful in preventing muscle fibrosis after denervation. In this study, we examined the relationships between miR-21 expression and fibrosis in vivo using mouse models and in vitro using the C2C12 cell line. Our results from the in vivo and in vitro experiments suggested that miR-21 promoted fibrosis by targeting TGF-β/Smad7-Smad2/3 signaling pathway. However, this study has some limitations. For example, although the miRNA microarray showed that several miRNAs were involved in fibrosis, including miR-21, miR-744, miR-663, miR-15a, and miR-424, we focused on miR-21. Furthermore, although the TGF-β1/SMAD signaling pathway plays an important role in fibrogenesis, we did not consider other signaling pathways that play a role in gastrocnemius muscle atrophy and fibrosis. Further research is needed to elucidate the mechanisms of gastrocnemius muscle fibrosis.

5. Conclusion

In summary, the present study elucidates the role of miR-21 in regulating the TGF beta/Smad signaling pathway of myoblast fibrogenesis. The results demonstrated that miR-21 promoted myoblast fibrogenesis via targeting Smad7. Our results may provide a promising therapeutic target for skeletal muscle fibrosis.

Ethics approved and consent to participate

All experimental procedures were approved by the Institutional Animal Care and Use Committee at Second Military Medical University and adhered to associated guidelines on the ethical use of animals (CHEC-2022-046) .

Funding

This work was supported by Grant Nos. 81970868, 81570905, and 81400474 for science research from the National Natural Science Foundation of China.

Declaration of generative AI in scientific writing

The authors declare no AI in scientific writing.

CRediT authorship contribution statement

Xianmin Song: Writing – original draft, Methodology, Funding acquisition, Conceptualization. **Fei Liu:** Writing – original draft, Supervision, Data curation. **Mengjie Chen:** Visualization, Investigation. **Minhui Zhu:** Formal analysis, Data curation. **Hongliang Zheng:** Validation, Funding acquisition. **Wei Wang:** Project administration, Methodology. **Donghui Chen:** Writing – review &

editing, Conceptualization. **Meng Li:** Writing – review & editing, Conceptualization. **Shicai Chen:** Writing – review & editing, Funding acquisition, Conceptualization.

Declaration of competing interest

The authors declare the following financial interests/personal relationships which may be considered as potential competing interests: ShicaiChen reports financial support was provided by National Natural Science Foundation of China. Hongliang Zheng reports financial support was provided by National Natural Science Foundation of China. Xianmin Song reports financial support was provided by National Natural Science Foundation of China. If there are other authors, they declare that they have no known competing financial interests or personal relationships that could have appeared to influence the work reported in this paper.

Appendix A. Supplementary data

Supplementary data to this article can be found online at https://doi.org/10.1016/j.heliyon.2024.e33062.

References

[1] H. Zheng, et al., Update: laryngeal reinnervation for unilateral vocal cord paralysis with the ansa cervicalis, Laryngoscope 106 (12 Pt 1) (1996) 1522–1527.
[2] A. Guclu, et al., Micro RNA-320 as a novel potential biomarker in renal ischemia reperfusion, Ren. Fail. 38 (9) (2016) 1468–1475.
[3] J. Batt, et al., Differential gene expression profiling of short and long term denervated muscle, Faseb. J. 20 (1) (2006) 115–117.
[4] J. Huard, Y. Li, F.H. Fu, Muscle injuries and repair: current trends in research, J Bone Joint Surg Am 84 (5) (2002) 822–832.
[5] R.L. Lieber, S.R. Ward, Cellular mechanisms of tissue fibrosis. 4. Structural and functional consequences of skeletal muscle fibrosis, Am. J. Physiol. Cell Physiol. 305 (3) (2013) C241–C252.
[6] Y. Liu, E. Dai, J. Yang, Quercetin suppresses glomerulosclerosis and TGFbeta signaling in a rat model, Mol. Med. Rep. 19 (6) (2019) 4589–4596.
[7] F. Accornero, et al., Genetic analysis of connective tissue growth factor as an effector of transforming growth factor beta signaling and cardiac remodeling, Mol. Cell Biol. 35 (12) (2015) 2154–2164.
[8] D.L. Allen, D.H. Teitelbaum, K. Kurachi, Growth factor stimulation of matrix metalloproteinase expression and myoblast migration and invasion in vitro, Am. J. Physiol. Cell Physiol. 284 (4) (2003) C805–C815.
[9] C. Vial, et al., Skeletal muscle cells express the profibrotic cytokine connective tissue growth factor (CTGF/CCN2), which induces their dedifferentiation, J. Cell. Physiol. 215 (2) (2008) 410–421.
[10] F. Liu, et al., Expression of TGF-beta1 and CTGF is associated with fibrosis of denervated sternocleidomastoid muscles in mice, Tohoku J. Exp. Med. 238 (1) (2016) 49–56.
[11] H.Y. Meng, L.Q. Chen, L.H. Chen, The inhibition by human MSCs-derived miRNA-124a overexpression exosomes in the proliferation and migration of rheumatoid arthritis-related fibroblast-like synoviocyte cell, BMC Muscoskel. Disord. 21 (1) (2020) 150.
[12] Q. Li, et al., Human keratinocyte-derived microvesicle miRNA-21 promotes skin wound healing in diabetic rats through facilitating fibroblast function and angiogenesis, Int. J. Biochem. Cell Biol. 114 (2019) 105570.
[13] G.E. Melling, et al., A miRNA-145/TGF-beta1 negative feedback loop regulates the cancer-associated fibroblast phenotype, Carcinogenesis 39 (6) (2018) 798–807.
[14] S. Chen, et al., miR-491-5p inhibits Emilin 1 to promote fibroblasts proliferation and fibrosis in gluteal muscle contracture via TGF-Beta1/Smad2 pathway, Physiol. Res. 71 (2) (2022) 285–295.
[15] X.L. Zhou, et al., miR-21 promotes cardiac fibroblast-to-myofibroblast transformation and myocardial fibrosis by targeting Jagged 1, J. Cell Mol. Med. 22 (8) (2018) 3816–3824.
[16] J. Yuan, et al., Mir-21 promotes cardiac fibrosis after myocardial infarction via targeting Smad7, Cell. Physiol. Biochem. 42 (6) (2017) 2207–2219.
[17] S. Zafar, et al., Calotropis procera (leaves) supplementation exerts curative effects on promoting functional recovery in a mouse model of peripheral nerve injury, Food Sci. Nutr. 9 (9) (2021) 5016–5027.
[18] C. Linard, et al., Long-term effectiveness of local BM-MSCs for skeletal muscle regeneration: a proof of concept obtained on a pig model of severe radiation burn, Stem Cell Res. Ther. 9 (1) (2018) 299.
[19] A.P. Valencia, et al., Impaired contractile function of the supraspinatus in the acute period following a rotator cuff tear, BMC Muscoskel. Disord. 18 (1) (2017) 436.
[20] C.J. Mann, et al., Aberrant repair and fibrosis development in skeletal muscle, Skeletal Muscle 1 (1) (2011) 21.
[21] W. Sulaiman, T. Gordon, Neurobiology of peripheral nerve injury, regeneration, and functional recovery: from bench top research to bedside application, Ochsner J. 13 (1) (2013) 100–108.
[22] J. Hanna, G.S. Hossain, J. Kocerha, The potential for microRNA therapeutics and clinical research, Front. Genet. 10 (2019) 478.
[23] S.E. Meyer, MicroRNA immunomodulating therapeutics, Blood 135 (3) (2020) 155–156.
[24] K. Lundstrom, Micro-RNA in disease and gene therapy, Curr. Drug Discov. Technol. 8 (2) (2011) 76–86.
[25] T.L.E. van Westering, et al., Uniform sarcolemmal dystrophin expression is required to prevent extracellular microRNA release and improve dystrophic pathology, J Cachexia Sarcopenia Muscle 11 (2) (2020) 578–593.
[26] G. Xiong, et al., Inhibition of microRNA-21 decreases the invasiveness of fibroblast-like synoviocytes in rheumatoid arthritis via TGFbeta/Smads signaling pathway, Iran J Basic Med Sci 19 (7) (2016) 787–793.
[27] P. Wang, et al., miR-21 in EVs from pulmonary epithelial cells promotes myofibroblast differentiation via glycolysis in arsenic-induced pulmonary fibrosis, Environ. Pollut. 286 (2021) 117259.
[28] W. Li, et al., HBV induces liver fibrosis via the TGF-beta1/miR-21-5p pathway, Exp. Ther. Med. 21 (2) (2021) 169.
[29] J.R. Liu, et al., Caloric restriction alleviates aging-related fibrosis of kidney through downregulation of miR-21 in extracellular vesicles, Aging (Albany NY) 12 (18) (2020) 18052–18072.
[30] H. Guo, et al., miR-21 is upregulated, promoting fibrosis and blocking G2/M in irradiated rat cardiac fibroblasts, PeerJ 8 (2020) e10502.
[31] B. Moreira Soares Oliveira, M. Durbeej, J. Holmberg, Absence of microRNA-21 does not reduce muscular dystrophy in mouse models of LAMA2-CMD, PLoS One 12 (8) (2017) e0181950.
[32] T. Makiguchi, et al., Serum extracellular vesicular miR-21-5p is a predictor of the prognosis in idiopathic pulmonary fibrosis, Respir. Res. 17 (1) (2016) 110.
[33] J. Zhang, et al., miR-21 inhibition reduces liver fibrosis and prevents tumor development by inducing apoptosis of CD24+ progenitor cells, Cancer Res. 75 (9) (2015) 1859–1867.
[34] T. Thum, et al., Comparison of different miR-21 inhibitor chemistries in a cardiac disease model, J. Clin. Invest. 121 (2) (2011) 461–462, author reply 462-463.

[35] D.M. Patrick, et al., Stress-dependent cardiac remodeling occurs in the absence of microRNA-21 in mice, J. Clin. Invest. 120 (11) (2010) 3912–3916.
[36] J. Wang, et al., Resveratrol inhibits pulmonary fibrosis by regulating miR-21 through MAPK/AP-1 pathways, Biomed. Pharmacother. 105 (2018) 37–44.
[37] Y. Wang, et al., Antischistosomiasis liver fibrosis effects of chlorogenic acid through IL-13/miR-21/smad7 signaling interactions in vivo and in vitro, Antimicrob. Agents Chemother. 61 (2) (2017).
[38] Q. Huang, et al., Methyl helicterte ameliorates liver fibrosis by regulating miR-21-mediated ERK and TGF-beta1/Smads pathways, Int. Immunopharm. 66 (2019) 41–51.
[39] J. Guo, Effect of miR-21 on renal fibrosis induced by nano-SiO(2) in diabetic nephropathy rats via PTEN/AKT pathway, J. Nanosci. Nanotechnol. 21 (2) (2021) 1079–1084.
[40] K.C. Yang, et al., Combined deep microRNA and mRNA sequencing identifies protective transcriptomal signature of enhanced PI3Kalpha signaling in cardiac hypertrophy, J. Mol. Cell. Cardiol. 53 (1) (2012) 101–112.
[41] H. Cui, et al., Macrophage-Derived miRNA-containing exosomes induce peritendinous fibrosis after tendon injury through the miR-21-5p/smad7 pathway, Mol. Ther. Nucleic Acids 14 (2019) 114–130.
[42] J.Y. Lai, et al., MicroRNA-21 in glomerular injury, J. Am. Soc. Nephrol. 26 (4) (2015) 805–816.
[43] L. Lin, et al., MicroRNA-21 inhibits SMAD7 expression through a target sequence in the 3' untranslated region and inhibits proliferation of renal tubular epithelial cells, Mol. Med. Rep. 10 (2) (2014) 707–712.
[44] Q. Li, et al., MiR-21/Smad 7 signaling determines TGF-beta1-induced CAF formation, Sci. Rep. 3 (2013) 2038.
[45] H.Y. Lan, Smad7 as a therapeutic agent for chronic kidney diseases, Front. Biosci. 13 (2008) 4984–4992.
[46] W. Sun, et al., Renoprotective effects of maslinic acid on experimental renal fibrosis in unilateral ureteral obstruction model via targeting MyD88, Front. Pharmacol. 12 (2021) 708575.
[47] J. Zeng, et al., Inhibition of sphingosine kinase 2 attenuates hypertrophic scar formation via upregulation of Smad7 in human hypertrophic scar fibroblasts, Mol. Med. Rep. 22 (3) (2020) 2573–2582.
[48] A.C. Chung, et al., Disruption of the Smad7 gene promotes renal fibrosis and inflammation in unilateral ureteral obstruction (UUO) in mice, Nephrol. Dial. Transplant. 24 (5) (2009) 1443–1454.
[49] K. Singh, et al., Arginyltransferase knockdown attenuates cardiac hypertrophy and fibrosis through TAK1-JNK1/2 pathway, Sci. Rep. 10 (1) (2020) 598, 2020. 10.
[50] F. Kong, M. Zhao, Loureirin B alleviates myocardial ischemia/reperfusion injury via inhibiting PAI-1/TGF-beta1/smad signaling pathway, Evid Based Complement Alternat Med 2022 (2022) 9128210.
[51] A.E. Jenike, M.K. Halushka, miR-21: a non-specific biomarker of all maladies, Biomark. Res. 9 (1) (2021) 18.